Supplement of

Impact of International Shipping Emissions on Ozone and PM$_{2.5}$: The Important Role of HONO and ClNO$_2$

Jianing Dai[1], Tao Wang[1]

Department of Civil and Environmental Engineering, The Hong Kong Polytechnic University, Hong Kong, 999077, China

Correspondence to: Tao Wang (cetwang@polyu.edu.hk)

Number of pages: 17

Number of tables: 4

Number of figures: 11

Table S1. Ranges of latitude and longitude in nine regions.

Regions	Ranges of latitude	Ranges of longitude
South China Sea (SCS)	0—25°N	100°E—125°E
East China Sea (ECS)	25°N—35°N	119°E—130°E
Bohai Rim (BR)	35°N—41°N	118°E—127°E
Bay of Bengal (BOB)	10°N—25°N	80°E—95°E
The Sea of Japan (SOJ)	35°N—50°N	130°E—142°E
West Pacific Ocean (WPO)	0—35°N	125°E—142°E

Table S2. Statistics of meteorological variables and air pollutants.

	OBS [a]	SIM [a]	MB [b]	NMB [b] (%)	NME [b] (%)	R [b]
WS_{10} [c] (m s^{-1})	4.5	5.3	0.8	1.0	1.2	0.90
RH [c] (%)	80.2	82.0	2.0	2.2	2.4	0.94
T_2 [c] (°C)	28.4	29.0	0.6	0.8	1.2	0.88
$PM_{2.5}$ [d] (µg m^{-3})	45.2	55.8	17.6	18.7	20.0	0.42
NO_2 [d] (ppbv)	13.8	10.5	-3.3	-8.5	10.0	0.61
Ozone [d] (ppbv)	83.3	77.8	-5.5	-8.7	12.4	0.77

[a] SIM is the simulated data, OBS is the observational data.

[b] Mean Bias $(MB) = \frac{\sum_{i=1}^{n}(x_i - y_i)}{n}$; Normalized Mean Bias $(NMB) = \sum_{i=1}^{n} \frac{Sim_i - Obs_i}{Obs_i}$; Normalized

Mean Errors $(NME) = \sum_{i=1}^{n} \frac{|Sim_i - Obs_i|}{Obs_i}$; $R = \frac{\sum_{i=1}^{n}(x_i - \bar{x})(y_i - \bar{y})}{\sqrt{\sum_{i=1}^{n}(x_i - \bar{x})^2 \sum_{i=1}^{n}(y_i - \bar{y})^2}}$; n is the number of hour.

[c] Observational data was obtained from the National Climate Data Center (NCDC). WS_{10}: wind speed at 10 m; T_2: temperature at 2 m; RH: specific humidity at 2 m.

[d] Observational data was obtained from China's Ministry of Ecology and Environment (MEE).

Table S3. Statistics of model performance in different cases for hourly O_3 measurements at MEE station and monthly O_3 in three marine sites (Unit: ppbv).

Regions	CASE	OBS	SIM	MB
HT[a]	Default		19.6	-2.8
	HONO	22.4	20.3	-2.1
	Cl		19.9	-2.5
	BASE		20.9	-1.5
Ryori	Default		21.3	-4.8
	HONO		23.1	-3.0
	Cl	26.1	22.1	-4.0
	BASE		24.1	-2.0
Yona[b]	Default		17.6	-2.3
	HONO		19.2	-0.7
	Cl	19.9	18.6	-1.3
	BASE		19.2	-0.7

[a] North Central Plain (NCP), [b]Yangzi River Delta (YRD), [c] Pearl River Delta (PRD), [d] Hok Tsui (HT), [e] Yonagunijima (Yona).

Table S4. Comparison between simulated and observed HONO, N_2O_5, and $ClNO_2$ in coastal and marine sites.

Species	Location	Sites type	Observational period	Observational average	References
HONO	South of Vancouver	Coastal site	25 July to 8 August 2008	0.5-1.5 ppbv	Wojtal et al. (2011)
	North Atlantic Ocean	Marine site	5 July and 8 July 2013	8.8-11.3 pptv	Ye et al. (2016)
	Mediterranean island	Coastal remote site	7 July to 4 August 2014	35.0 pptv	Meusel et al. (2016)
	Eastern Bohai Sea	Marine background site	5 October to 5 November 2016	0.2 ppbv	Wen et al. (2019)
	Eastern Atlantic Ocean	Marine background site	24 November and 3 December 2015	3.0-6.0 pptv	Kasibhatla et al. (2018)
	East China Sea	Shipboard-based measurement	July 2017	0.6-1.1 ppbv	Cui et al. (2019)
	South China Sea	Coastal background site	31 August to 8 October 2018	89.0 pptv [a]	Unpublished data
N_2O_5	South China Sea	Coastal background site	31 August to 8 October 2018	8.5 pptv [a]	Unpublished data
$ClNO_2$	South China Sea	Coastal background site	31 August to 8 October 2018	89.0 pptv [a]	Unpublished data

[a] Observed data was filtered with one-day backward trajectory from ocean.
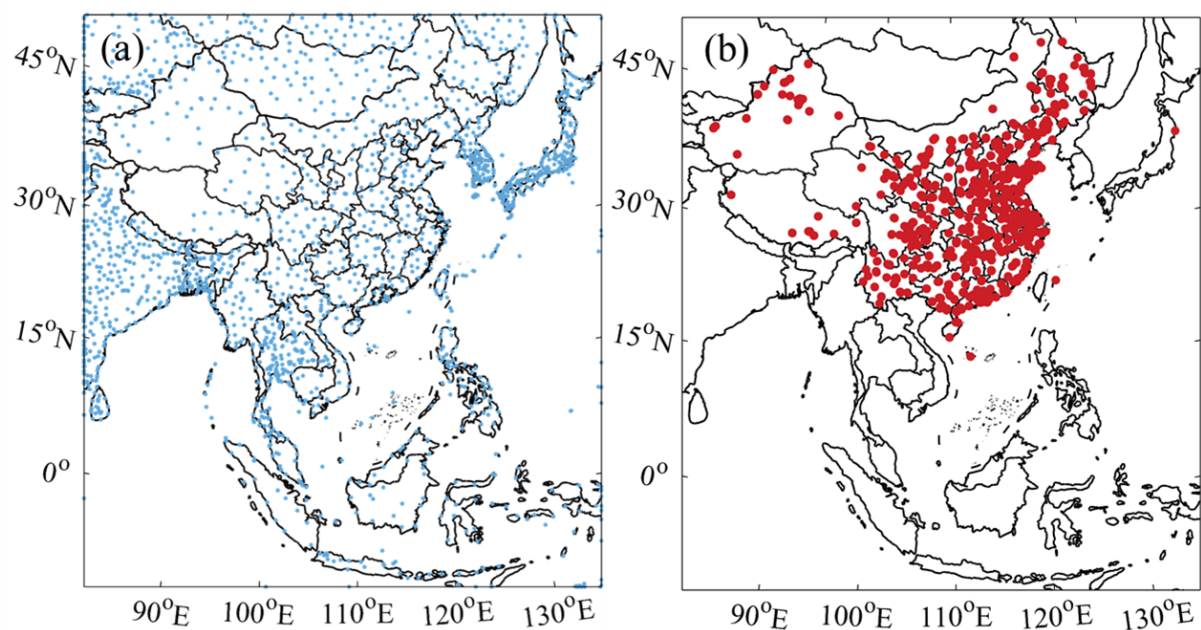
Figure S1. Measurement sites. (a) Blue dots denote the surface weather stations in NCDC in July 2018. (b) Red dots denote the available surface air-quality monitoring stations operated by MEE in July 2018.
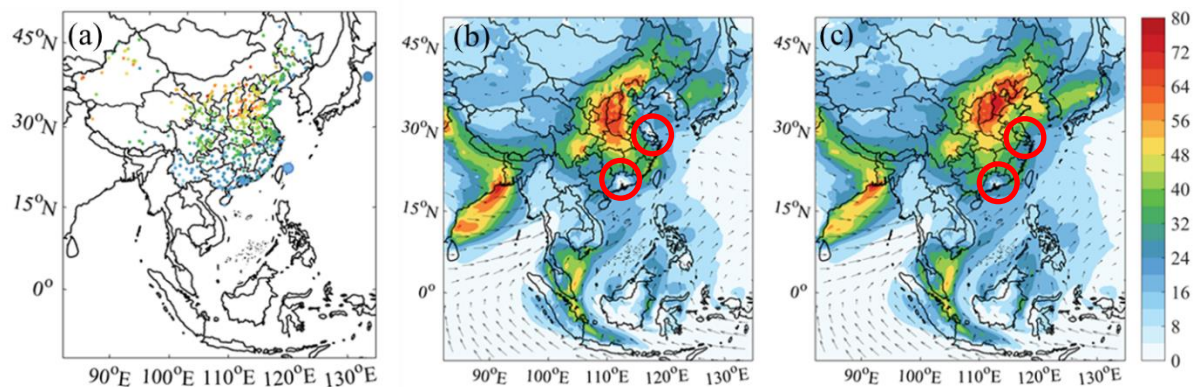
Figure S2. (a) Observations of O_3 at China MEE station and two marine sites in Japan and modeled O_3 mixing ratios with (b) default chemistry and (c) integrated HONO and chlorine chemistry (Unit: ppbv). The red circles in (b) and (c) highlight the O_3 simulation in coastal areas.
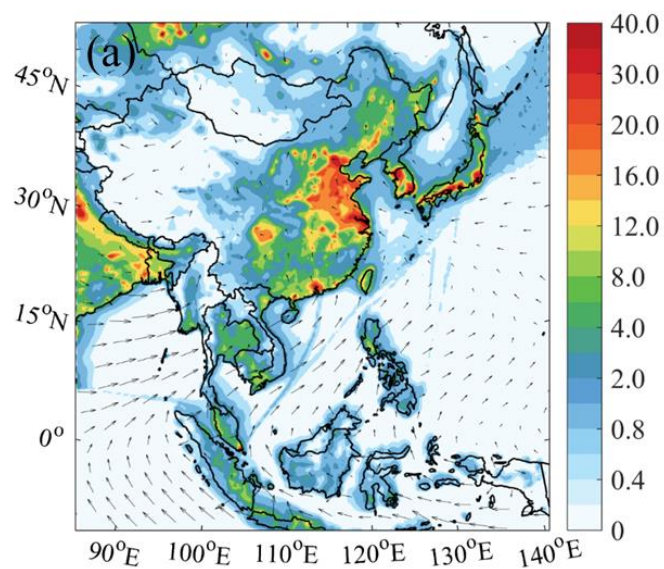
Figure S3. (a) Spatial distribution of averaged NO$_2$ (Unit: ppbv) at the surface. Arrows present the simulated wind vectors from the BASE case.
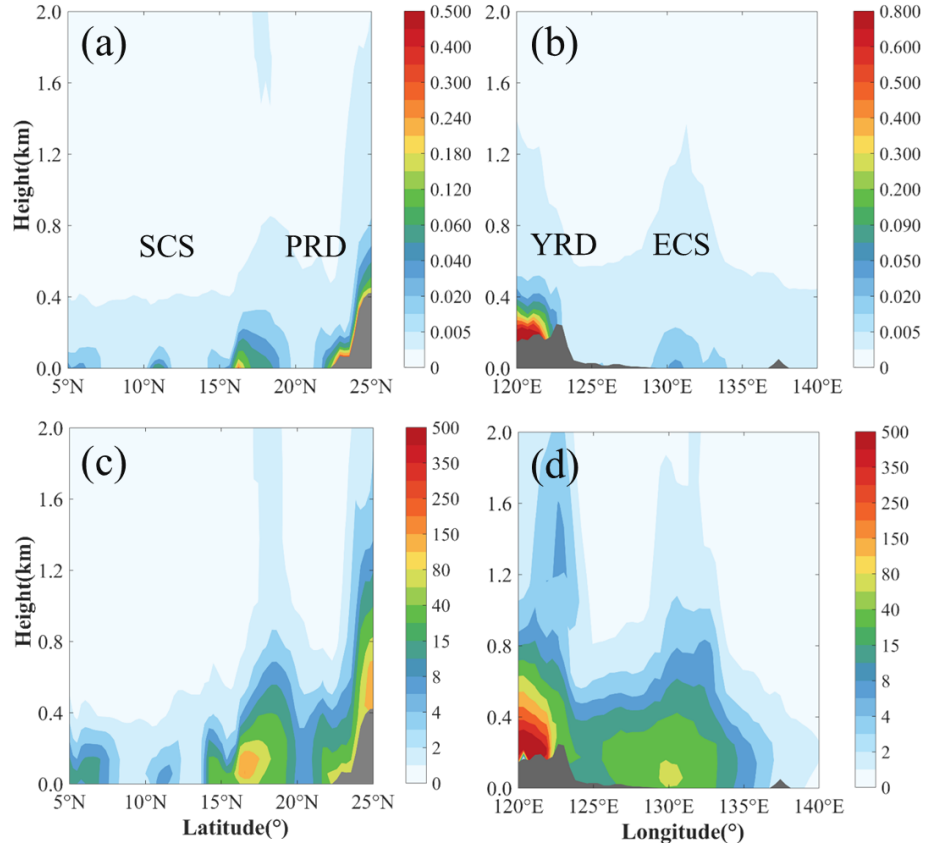
Figure S4. Vertical distribution of averaged (a)(b) HONO (Unit: ppbv) and (c)(d) nighttime ClNO$_2$ (Unit: pptv) at cross-section by 113°E and 31°N, respectively in July 2018 from the BASE case. Arrows and the gray shadow present the topography high from the BASE case. We also highlight the South China Sea (SCS) and Pearl River Delta (PRD) in (a) and Yangzi River Delta (YRD) and East China Sea (ECS) in (b).
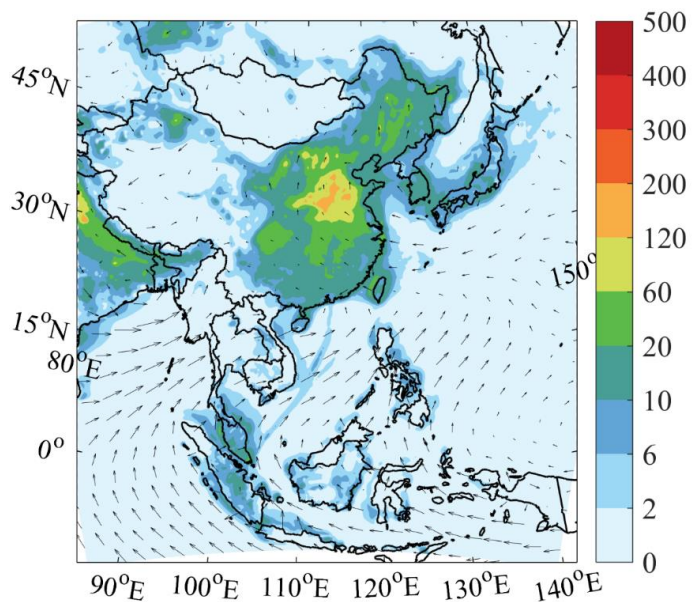
Figure S5. Spatial distribution of averaged N_2O_5 (Unit: pptv) during nighttime (18:00-06:00 LST) at the surface from the BASE case in July 2018. Arrows present the simulated wind vectors from the BASE case.
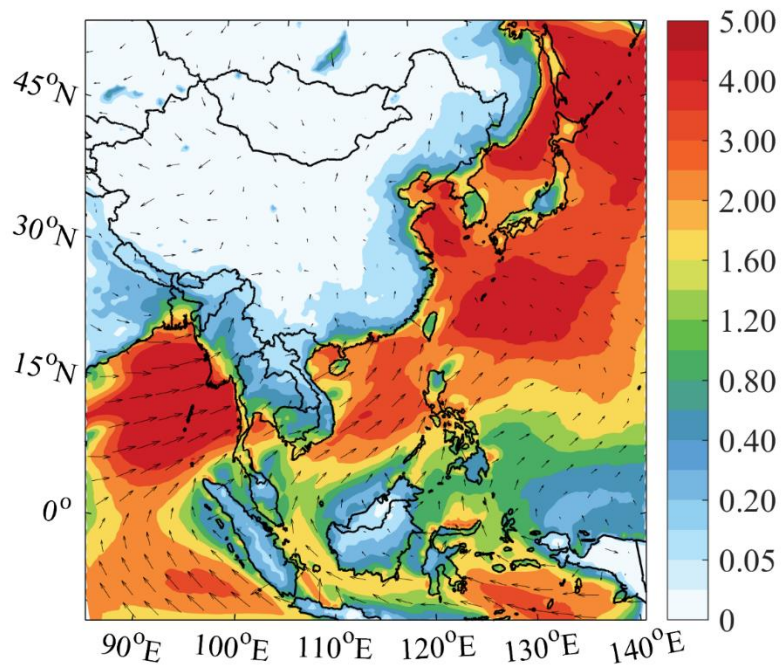
Figure S6. Spatial distribution of averaged fine particulate chloride (Unit: μg m^{-3}) at the surface from the BASE case in July 2018. Arrows present the simulated wind vectors from the BASE case.
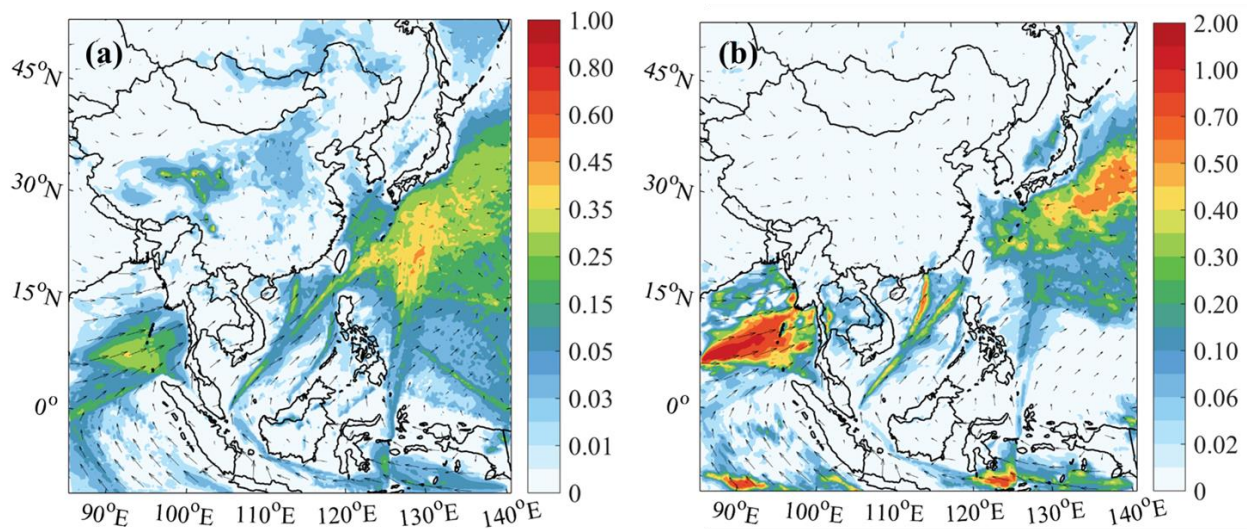
Figure S7. Average variation of simulated (a) OH radical (Unit: pptv) during daytime from the ship emission with additional HONO chemistry (HONO - HONO_noship) and (b) Cl radical (Unit:10^{-9} pptv) during daytime from the ship emission with chlorine chemistry (Cl - Cl_noship).
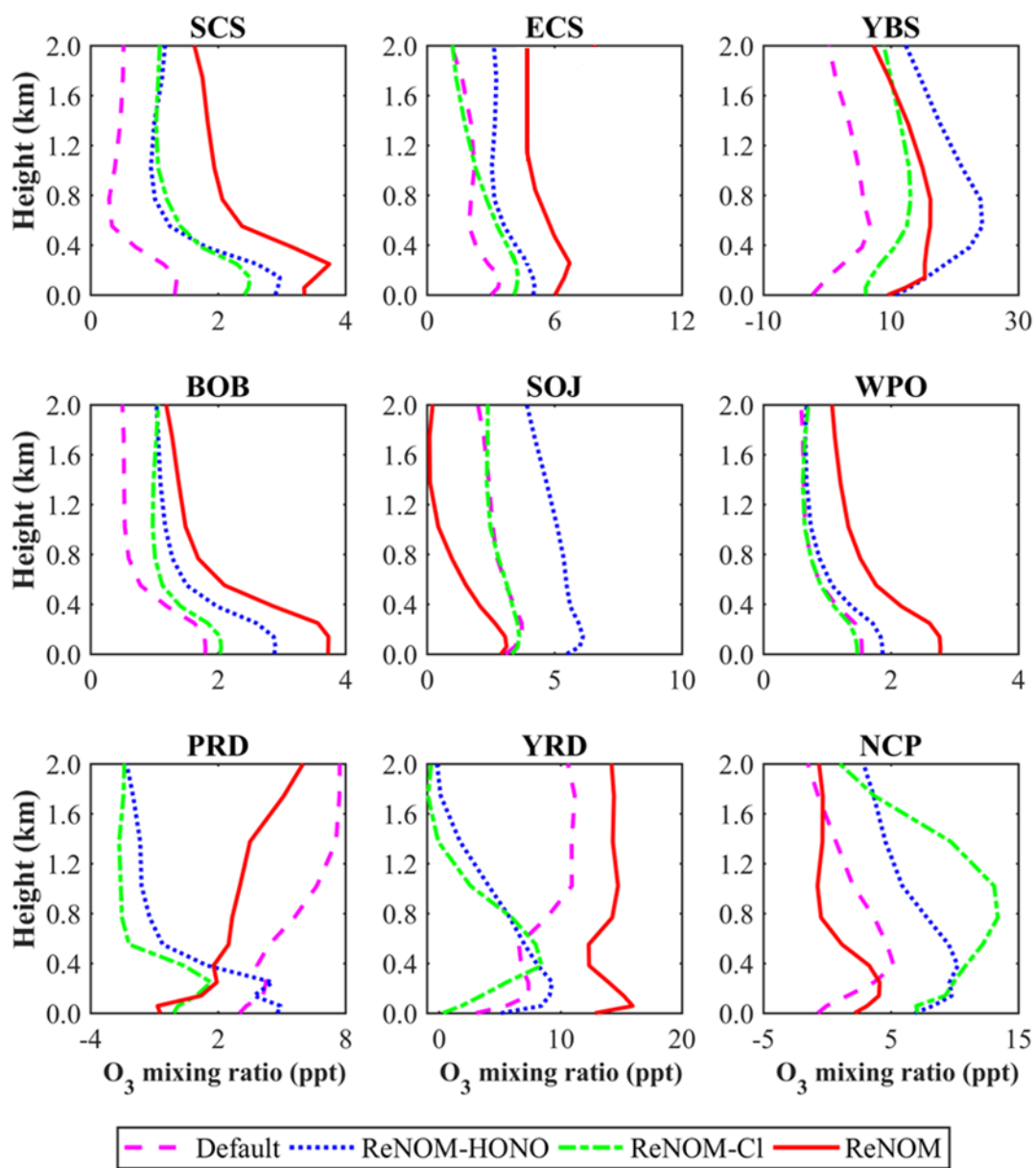
Figure S8. Vertical profiles of O$_3$ variations (Unit: ppbv) from different chemistry in nine regions.
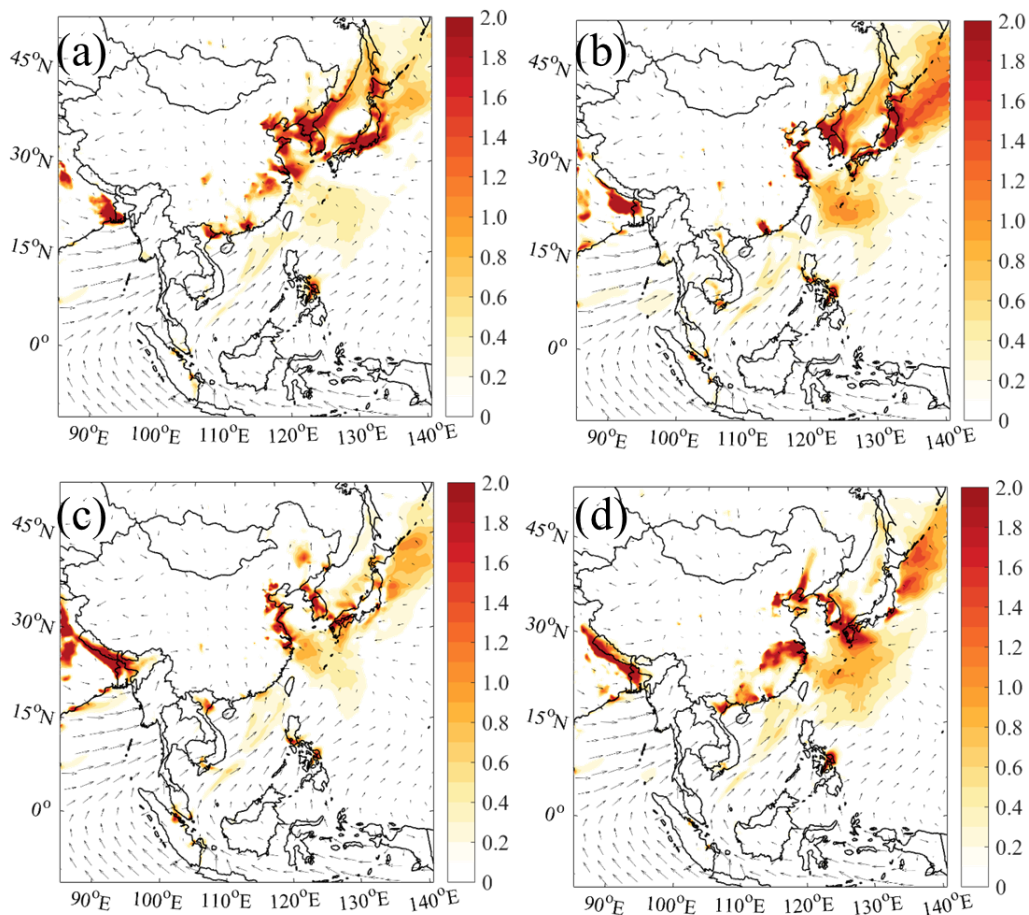
Figure S9. Averaged fine particulate nitrate enhancement (Unit: $\mu g\,m^{-3}$) with (a) default chemistry (Def-Def_noship), (b) default and additional HONO chemistry (HONO-HONO_noship), (c) default and additional chlorine chemistry (Cl-Cl_noship) and (d) default and integrated HONO and chlorine chemistry (BASE-BASE_noship). Arrows present the simulated wind vectors from the BASE case.
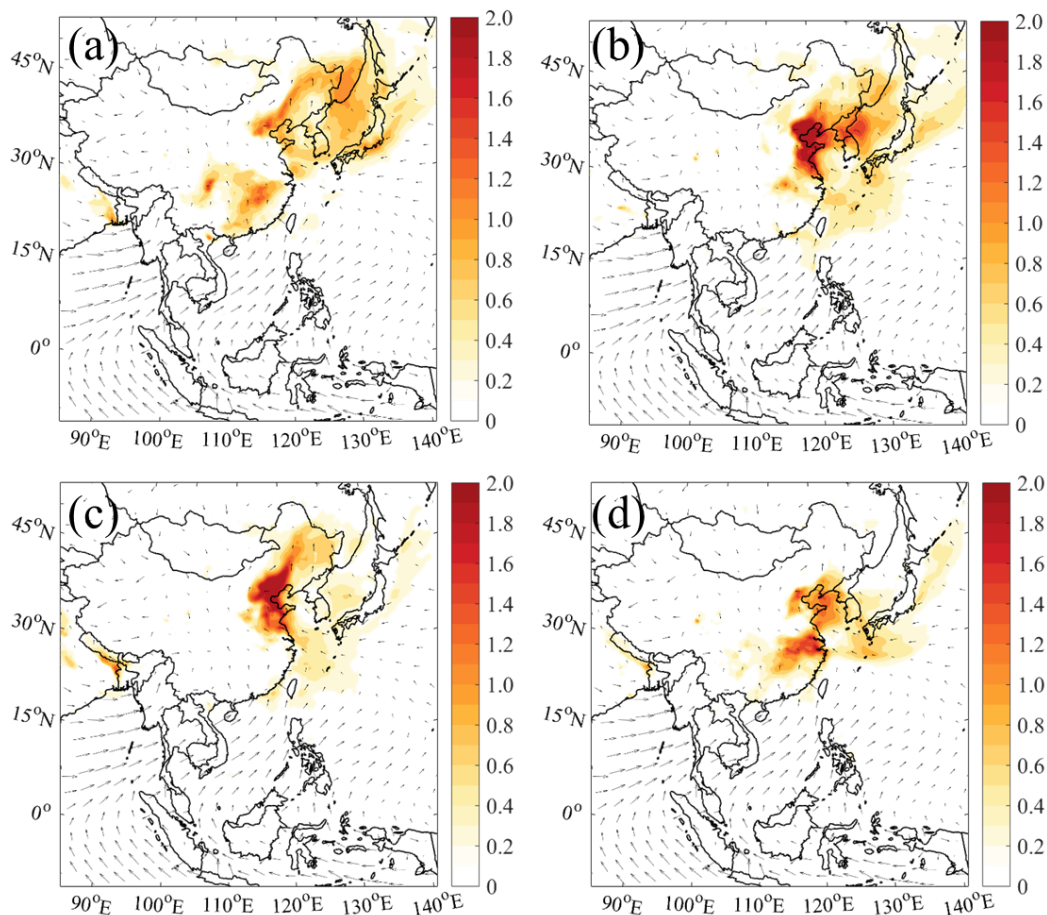
Figure S10. Averaged fine particulate sulfur enhancement (Unit: μg m^{-3}) with (a) default chemistry (Def-Def_noship), (b) default and additional HONO chemistry (HONO-HONO_noship), (c) default and additional chlorine chemistry (Cl-Cl_noship) and (d) default and integrated HONO and chlorine chemistry (BASE-BASE_noship). Arrows present the simulated wind vectors from the BASE case.
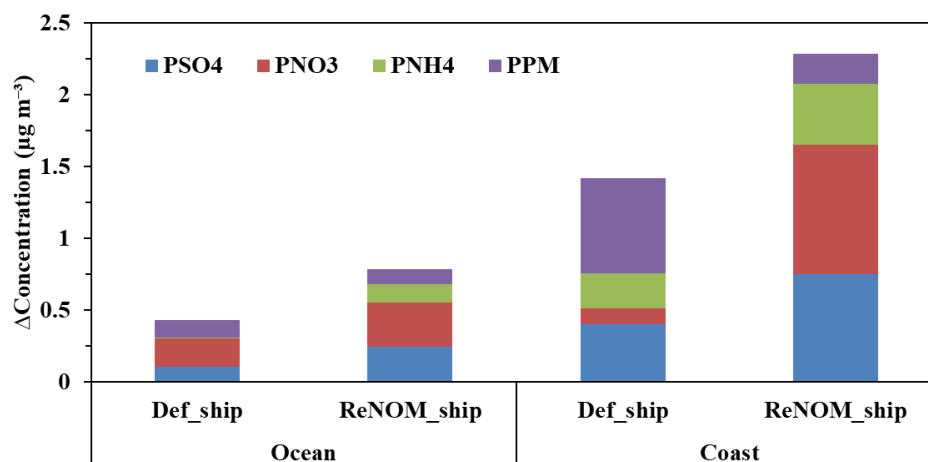
Figure S11. Contribution of ship emission to the concentration of detailed aerosol species in oceanic areas and coastal cities. PSO4, PNO3, PNH4 and PPM represent the fine particulate sulfate, fine particulate nitrate, fine particulate ammonia, and primary particulate matter, respectively. Def_ship and ReNOM_ship represents Def-Def_noship and BASE-BASE_noship, respectively.

References

CUI, L., LI, R., FU, H., LI, Q., ZHANG, L., GEORGE, C. & CHEN, J. 2019. Formation features of nitrous acid in the offshore area of the East China Sea. *Science of The Total Environment,* 682**,** 138-150.

KASIBHATLA, P., SHERWEN, T., EVANS, M. J., CARPENTER, L. J., REED, C., ALEXANDER, B., CHEN, Q., SULPRIZIO, M. P., LEE, J. D. & READ, K. A. 2018. Global impact of nitrate photolysis in sea-salt aerosol on NOx, OH, and O3 in the marine boundary layer. *Atmospheric Chemistry and Physics***,** 11185-11203.

MEUSEL, H., KUHN, U., REIFFS, A., MALLIK, C., HARDER, H., MARTINEZ, M., SCHULADEN, J., BOHN, B., PARCHATKA, U. & CROWLEY, J. N. 2016. Daytime formation of nitrous acid at a coastal remote site in Cyprus indicating a common ground source of atmospheric HONO and NO. *Atmospheric Chemistry and Physics,* 16**,** 14475-14493.

WEN, L., CHEN, T., ZHENG, P., WU, L., WANG, X., MELLOUKI, A., XUE, L. & WANG, W. 2019. Nitrous acid in marine boundary layer over eastern Bohai Sea, China: Characteristics, sources, and implications. *Science of the total environment,* 670**,** 282-291.

WOJTAL, P., HALLA, J. & MCLAREN, R. 2011. Pseudo steady states of HONO measured in the nocturnal marine boundary layer: a conceptual model for HONO formation on aqueous surfaces. *Atmospheric Chemistry and Physics,* 11**,** 3243.

YE, C., ZHOU, X., PU, D., STUTZ, J., FESTA, J., SPOLAOR, M., TSAI, C., CANTRELL, C., MAULDIN, R. L. & CAMPOS, T. 2016. Rapid cycling of reactive nitrogen in the marine boundary layer. *Nature,* 532**,** 489-491.